# Electrode pattern definition in ultrasound power transfer systems $\odot$

Moustafa Sayed Ahmed ; Shima Shahab ■



Appl. Phys. Lett. 122, 124101 (2023) https://doi.org/10.1063/5.0139866





CrossMark

# Articles You May Be Interested In

Mode couplings in multiplex electromechanical structures

Journal of Applied Physics (September 2022)





# Electrode pattern definition in ultrasound power transfer systems 🐵

Cite as: Appl. Phys. Lett. 122, 124101 (2023); doi: 10.1063/5.0139866 Submitted: 23 December 2022 · Accepted: 3 March 2023 · Published Online: 20 March 2023







Moustafa Sayed Ahmed (b) and Shima Shahabal (b)



### **AFFILIATIONS**

Department of Mechanical Engineering, Virginia Tech, Blacksburg, Virginia 24061, USA

a) Author to whom correspondence should be addressed: sshahab@vt.edu

#### ABSTRACT

We use a high pattern-fidelity technique on piezoelectric electrodes to selectively excite high-order vibration modes, while isolating other modes, in multi-layered through-wall ultrasound power transfer (TWUPT) systems. Physical mechanisms, such as direct and inverse piezoelectric effects at transmitting and receiving piezoelectric elements, as well as wave propagation across an elastic barrier and coupling layers, all contribute to TWUPT. High-order radial modes in a TWUPT system feature strain nodes, where the dynamic strain distribution changes sign in the direction of disks' radii. This study explains theoretically and empirically how covering the strain nodes of vibration modes with continuous electrodes results in substantial cancelations of the electrical outputs. A detailed analysis is given for predicting the locations of the strain nodes. The electrode patterning for creating the transmitter and receiver shapes is determined by the regions where local force and charge cancelation do not occur, i.e., the two modal principal stress components have the same sign. Patterning for creating the electrode shapes is performed by high-fidelity numerical modeling supported by experiments. Using differential excitation on the transmitter side while monitoring transmitted power and efficiency on the reception side at various vibration modes is made possible by the unique nature of TWUPT systems. Due to an improvement in system quality and power factors, it is determined that employing the proposed electrode pattern designs enhances overall device efficiency and active power. The suppression of other modes makes up a filter feature that is paired with the enhancement at the mode under consideration.

Published under an exclusive license by AIP Publishing. https://doi.org/10.1063/5.0139866

Ultrasound power transfer (UPT) systems are a new prospective technology for wireless power delivery to difficult-to-reach components in essential engineering applications, 1,2 including medical ultrasound, where acoustic wave manipulation and focusing to confine acoustic intensity is of great importance.<sup>3–5</sup> The underlying mechanism of UPT systems involves the transmission of acoustic waves by a piezoelectric transmitter, propagating acoustic waves through a medium, and piezoelectric transduction of acoustic waves at a piezoelectric receiver. The received acoustic waves at the receiver end are usually used to power external attached circuits. The through-wall ultrasound power transfer (TWUPT) system is one type of UPT systems where the propagating medium is solid. TWUPT systems, which employ elastic barriers to propagate elastic longitudinal and shear waves, 6,7 are used for power and data transfer<sup>8,9</sup> as well as nondestructive evaluation.<sup>10</sup> As illustrated in Fig. 1(a), the TWUPT system comprises a transmitting piezoelectric element, an elastic wall, bonding layers, and a receiving piezoelectric element. The elastic layer allows for longitudinal and shear wave propagation, as well as direct and inverse piezoelectric transduction of elastic vibrations at the transmitting and receiving piezoelectric devices.

Electrical resistive loads are connected at the receiver end to measure the electric output (dissipated) power and efficiency (will be shown later in Fig. 6).

The fundamental natural frequency (thickness-extensional or radial mode) is frequently chosen for UPT systems due to its high quality factor and output (dissipated) power. UPT systems exhibit a limited response to high-order modes<sup>11–13</sup> because the full-electrode arrangement at the piezoelectric disk's surface is incapable of effectively activating these modes. Therefore, a wide range of various piezoelectric transducer sizes is needed to use UPT systems for higherfrequency applications. Achieving a compact integration of systems operating at multiple frequencies is significantly hampered by size constraints. As an alternative, the identical system's particular highorder vibration mode should be effectively and powerfully activated.

Systems involving piezoelectric disks that use high-order modes and successfully excite them have attracted interest in recent years. High-order modes have strain nodes along the thickness or radius (for disk shape) of piezoelectric (PZT, lead zirconate titanate) actuators and sensors, where the strain amplitude distribution

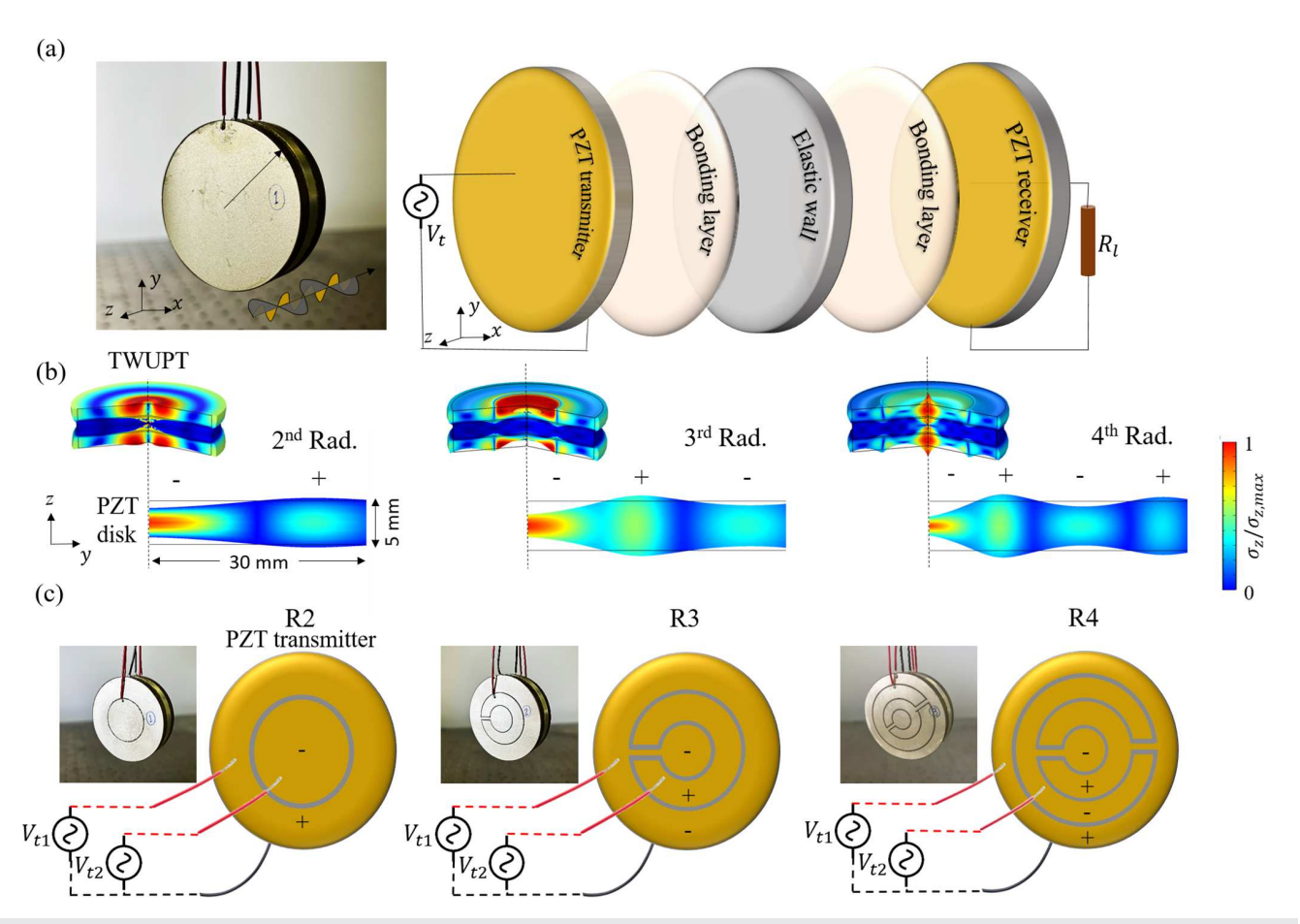


FIG. 1. (a) TWUPT system with piezoelectric disks in a full electrode configuration under free—free mechanical boundary conditions. The elastic wall enables direct and inverse piezoelectric transduction of elastic vibrations at the transmitting and receiving piezoelectric devices as well as longitudinal and shear wave propagation. To gauge the output (dissipated) power and efficiency of the electric system, electrical resistive loads are attached at the receiver end. (b) The 2D and 3D plots represent the stress distribution of a single piezoelectric disk and the corresponding TWUPT system calculated using FEM. The color bar represents the normalized absolute value of the z-component stress amplitude. The (+) and (-) symbols indicate induced positive and negative charges on the electrode surface resulting from mechanical tension and compression. (c) Three TWUPT systems with piezoelectric transmitters in different electrode pattern configurations. The transmitters are shown with the respective electrical connection. The piezoelectric transmitter and receiver are identical (same electrode pattern) and have a thickness of 5 mm and a radius of 30 mm. The two bonding layers are equivalent and have a thickness of 0.5 mm and a radius of 30 mm. The radius of the elastic wall is 30 mm and the thickness is 6 mm.

changes sign. The anti-nodes, i.e., maximum amplitude strain points, oscillate in opposition to one another with a 180° phase difference. Several approaches for electrode patterning have been applied to selectively activate some high-order modes while inhibiting others. 11 Pulskamp et al. 14 investigated the utilization of various electrode designs for arbitrary mode excitation in the PZT thin film on silicon radio frequency microelectromechanical systems plate, beam, ring, and disk resonators. They14 proposed using electrode shapes by identifying places where local force cancelation does not occur while leaving other sections un-electroded. As a result of their proposed technique, there are two alternative excitation electrode regions representing tensile and compressive zones, with one used for excitation and the other for detection. Although the technique demonstrated effective selective excitation results, differential excitation (opposite phase) of the two electrode locations might improve performance even further. Sanchez-Rojas et al. 19 considered differential excitation given to the two sections of the electrode shape. They<sup>19</sup> used surface displacement as a detection approach. The electrical impedance, output (dissipated) power, and efficiency are critical parameters to be considered for a thorough understanding of the influence of selective excitation on system behavior and so are better suited for detection.<sup>14</sup>

In this study, the use of differential excitation on the transmitter side while evaluating transmitted power and efficiency on the receiver side at various vibration modes is made possible by the particularity of through-wall ultrasound power transfer (TWUPT) systems. By using TWUPT systems, the challenges of measuring the effects on the system parameters and validating the electrode patterning technique are removed.

It is hypothesized that by applying electrode patterns to the piezoelectric electrodes of the transmitter and receiver in a TWUPT system, the desired vibration modes are enhanced and the undesirable modes are suppressed. Vibration modes are generally stimulated when

the piezoelectrically produced stresses match the modal stresses. <sup>14</sup> For instance, exciting regions of the piezoelectric element by locally applying compression forces will only strongly excite the natural modes that possess the same regions being under compression. The electrode patterning for the transmitter and receiver shapes is dictated by the locations where local force and charge cancelation does not occur, i.e., the two modal principal stress components have the same sign.

A finite element eigenfrequency study is implemented to identify the stress distribution of the second, third, and fourth radial modes. The compression (denoted as -), tension (denoted as +), and nodal regions of the considered modes are shown in Fig. 1(b). The disk operating at radial modes features radial distortion patterns in the lateral direction and grows in the thickness direction due to Poisson's ratio effects. The two regions in tension and compression (+ and -) oscillate in anti-phase (180° difference). Hence, the transmitter is driven in anti-phase (differential excitation) for strongly exciting the considered mode. For the third and fourth radial modes, referring to the stress distribution in Fig. 1(b), the electrode should be divided into three and four parts, respectively; two of which oscillate in phase. The continuous electrode is divided into + and - regions by removing electrode material from locations of the nodal circles. The two in-phase regions of the electrode are connected by extending a thin electrode as shown in Fig. 1(c). The electrode extension minimizes lead connections which comes at the price of force cancelation at the extended region. Figure 1(c) shows three TWUPT systems with distinct electrode pattern designs and piezoelectric transmitters. The electrical connections for the transmitters are illustrated. The 2D graphic depicts the FEMcalculated stress distribution of a single piezoelectric disk. The color bar represents the stress amplitude's normalized absolute value. Both the piezoelectric transmitter and receiver have the same electrode patterns.

There are a few modeling approaches for TWUPT, including the analytical method, <sup>6,7</sup> equivalent circuit method, <sup>20,21</sup> and finite element modeling (FEM) method. <sup>8,22,23</sup> Analytical and equivalent circuit modeling are two common one-dimensional modeling methodologies.

However, such a modeling method ignores the possibility of interaction between vibration modes at different transducer and receiver aspect ratios. In our earlier study, we used 2D axisymmetric FEM validated by experiments to examine the impact of mode couplings on the efficiency and active power of the TWUPT systems. It was demonstrated that mode couplings considerably affected the system quality factor and, as a result, the overall efficiency.

In this paper, we employ the FEM modeling approach as described in Ref. 8. The piezoelectric material properties are characterized using an optimization scheme in our prior study <sup>8,24</sup> and presented in Table I. The elastic constants, piezoelectric constants, and dielectric coefficients, as well as the elastic and bonding layer material properties, are listed in Table I. The losses in the TWUPT system were also properly characterized and incorporated in the model for accurate efficiency and power predictions. The epoxy quality factor is  $Q_b=7$ , the aluminum quality factor is  $Q_e=1000$ , and the average values of the piezoelectric mechanical and dielectric quality factors over the considered modes are  $Q_{P,m}=1800$  and  $Q_{P,d}=750$ , respectively.

In this work, high-order radial modes are used to operate the TWUPT systems. Radial mode devices are used in a variety of applications, including energy transfer<sup>8</sup> and piezoelectric converters. Because of the geometry of the piezoelectric disks used, the first radial mode has the lowest resonant frequency. As a result of the absence of spurious modes, a relatively clear frequency response can be obtained. Previously, we demonstrated that piezoelectric disks with an aspect ratio of d/t < 20 would be more efficient when operating near the radial mode rather than the thickness-extensional mode. The drop in efficiency is due to the interference of high-order vibration modes (mode couplings) near the thickness mode.

It is worth mentioning that thickness-extensional modes, unlike radial modes, have nodes and antinodes that grow along the material thickness rather than the electrode surface. As a result, electrode shaping for thickness-extensional modes is irrelevant. It is also important to note that in the presence of modes interference (coupling) and by using the designed electrode shape, the piezoelectrically produced

TABLE I. The material properties of the TWUPT system components. The properties are obtained using an optimization scheme in our prior study.8

			Piezo	electric d	isks					
Density (kg m $^{-3}$ ) $\rho$	Elastic (10 <sup>10</sup> Pa)					Piezoelectric (Cm <sup>-2</sup> )			Dielectric	
	$\overline{c_{11}^E}$	$c_{12}^E$	$c_{13}^E$	$c_{33}^{E}$	$c_{44}^E$	$\overline{e_{15}}$	$e_{31}$	e <sub>33</sub>	$\epsilon_{11}^S$	$\epsilon_{33}^{S}$
7650	15	7.8	8.05	13.1	2.564	12	-4.5	14.4	$680\epsilon_0$	550€
			Alur	ninum w	all					
Density (kg m <sup>-3</sup> )		Young's modulus (10 <sup>9</sup> Pa)					Poisson's ratio			
ho		E					v			
2710		69					0.33			
			Bonding	g layer (e	poxy)					
Density (kg m <sup>-3</sup> )		Young's modulus (10 <sup>9</sup> Pa)					Poisson's ratio			
ρ		E					v			
1150		4 (Avg)					0.35			

stresses will no more perfectly match the piezoelectric modal stresses allowing for local stress and charge cancelation. Therefore, in this study, we ensured that the considered wall dimensions avoid strong mode coupling at the operating frequencies.

Multiple measurements and numerical simulations are done to analyze the electrode patterning approach. The three TWUPT systems in different electrode configurations R2, R3, and R4 associated with the second, third, and fourth radial modes shown in Fig. 1(c) are tested and compared to the system in full electrode configuration. To address the physics of the TWUPT system, a 2D axisymmetric model with axisymmetric electrode patterns is used. The study employs proper sampling of the elastic waves at the given frequency range by assuming a free triangular mesh with an element size of (1/10  $\lambda_i$ ), where  $\lambda_i$  represents the acoustic wavelength in the ith domain. The FEM simulations are validated through experiments. A continuous sinusoidal wave at a certain frequency is used to stimulate the transmitter using a SIGLENT SDG1025 dual-output function generator. To the two electrode sections of the transmitter where anti-phase signals are applied, both function generator outputs are connected (differential excitation). On the receiver's side, the two electrode regions are shunted to two resistance substitution boxes, IET labs RS-2W. The input voltages,  $V_{t1}$ and  $V_{t2}$ , input currents (measured using Tektronix TCP2020),  $I_{t1}$  and  $I_{t2}$ , and output voltages,  $V_{r1}$  and  $V_{r2}$ , are measured using a Tektronix TBS20000B digital oscilloscope with 1 GHz sampling frequency. The efficiency is defined as  $\eta = \hat{P}_o/P_i$ , where  $P_o = V_{r1}^2/R_{11} + V_{r2}^2/R_{12}$  is the output power dissipated at the resistive loads,  $R_{11}$  and  $R_{12}$ , attached to the receiver and  $P_i = 1/2(|Re(V_{t1}I_{t1}^*)| + |Re(V_{t2}I_{t2}^*)|)$  is the input active power received by the transmitter. The asterisk denotes complex conjugate and Re denotes the real part of the complex number. The excitation voltage is fixed at 1 V amplitude for all numerical and experimental results. It should be noted that our tests, conducted at a low excitation level ( $V_{t1}=V_{t2}=1V$ ), demonstrate the TWUPT system's linear properties, where the amplitudes of the output voltage signals are proportional to the amplitudes of the input voltage signals. We note that the strains generated for 1 V voltage amplitude are insufficient to cause material nonlinear behavior in the TWUPT system layers. <sup>26,27</sup>

A key measure for analyzing the performance of the deployed electrode patterns is the system's efficiency. Figures 2(a)-2(c) represent FEM results for TWUPT systems employing R2, R3, and R4 electrode patterns shown in Fig. 1(c), respectively. Figures 2(d)-2(f) represent the experimental counterparts to Figs. 2(a)-2(c), respectively. The enhanced mode is shown in the highlighted area of each plot. The matching loads that maximize the efficiency are attached for each scenario assuming  $R_{l1} = R_{l2}$ . It should be noted that the applied electrode patterns on the transmitter and receiver improve system efficiency in the target mode. Electrode patterning, for instance, resulted in increases of 18%, 38%, and 42% at the target modes when R2, R3, and R4 electrode designs were used. In the experiment, this equates to an increase in 29%, 45%, and 40%. This is because electrode patterns avoid the cancelation of distributed forces at the excitation port and charge cancelation at the detection port, resulting in an increase in quality factor and output (dissipated) power.

We take the case study of applying the electrode patterns to either the receiver or transmitter alone in order to analyze the impact of each factor independently. In order to compare the three case studies, full electrode configuration on both ports (the conventional case), electrode patterns on both ports, and electrode

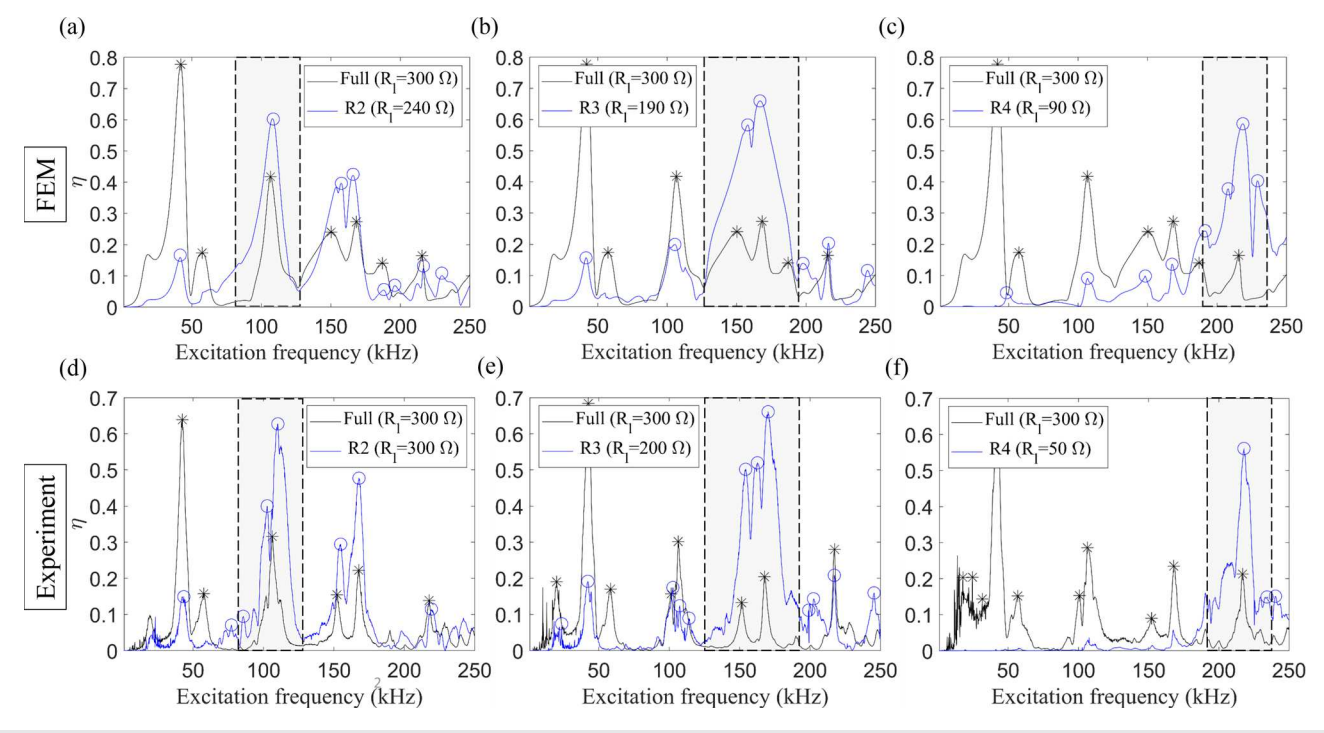
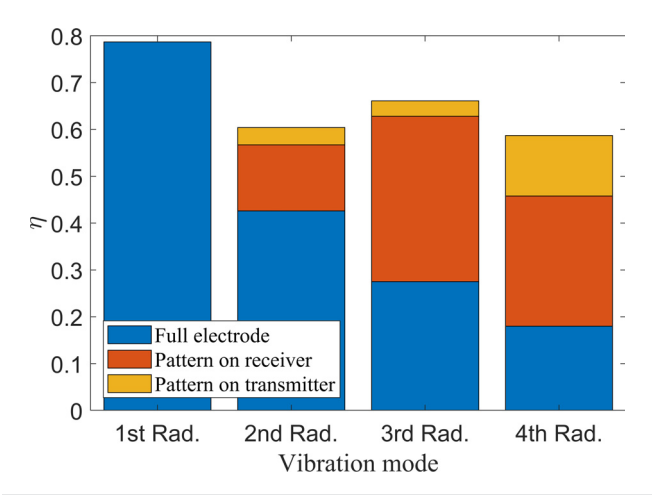


FIG. 2. Efficiency of the TWUPT system with regard to the excitation frequency. The plots in (a)–(c) show the FEM results, whereas (d)–(f) show the experimental results. The areas that are shaded display the modes of interest.



**FIG. 3.** TWUPT system's maximum efficiency near the first four radial modes by employing the three electrode patterns shown in Fig. 1(c), using FEM. There are three case studies considered: no electrode pattern applied (full electrode configuration), electrode patterns applied to the receiver only, and electrode patterns applied to the receiver and transmitter concurrently. The optimum matching loads (where  $R_{I1} = R_{I2}$ ) are considered for each case study.

pattern on the receiver while full electrode on the transmitter, are all used. The bar plot in Fig. 3 illustrates the outcomes of the case studies. As previously stated, the efficiency is calculated at equal attached matched loads ( $R_{l1} = R_{l2}$ ) in each case study. It is worth noting that the pattern on the receiver contributed to 14.1%, 35.3%, and 27.8% increase in the overall efficiency at the second, third, and fourth radial modes, respectively. This gain is due to the avoidance of charge cancelation at the receiver disk, which has a significant impact on the system's efficiency in all modes evaluated. Furthermore, using the electrode patterns on both ports demonstrates that the electrode pattern on the transmitter boosts

efficiency by 5.7%, 3.3%, and 13% at the second, third, and fourth radial modes, respectively. Force cancelation was avoided thanks to differential excitation used in the transmitter patterning, which raises the transducer's quality factor.

It is vital to highlight that efficiency is maximized by attaching matched loads that reduce wave reflections at the electric-acoustic channel port. 28 Two electrode areas (+ and -) represent two output ports of the electric-acoustic channel that must be tuned for the least reflections when using electrode patterns. The electrical input resistances  $(X_R)$  of the compression and tension regions [+ and - regions as ]shown in Fig. 1(b)] are not identical indicating a unique matching resistive load for each output port. A sweep of the attached loads,  $R_{l1}$ and  $R_{l2}$ , around the mode of interest demonstrates that the system efficiency can be further increased by adding distinct loads. The FEM results depicted in Fig. 4 show that the optimum attached loads are not identical for the three different electrode pattern configurations; R2, R3, and R4. In fact, the second, third, and fourth radial modes' efficiency is maximized at  $R_{l1}=380$  and  $R_{l2}=230$   $\Omega$ ,  $R_{l1}=210$  and  $R_{l2}=200~\Omega$ , and  $R_{l1}=30$  and  $R_{l2}=100~\Omega$ , respectively. It should also be observed that altering one of the resistive loads near the optimal levels has minimal influence on the system's efficiency. As a result, picking one of the attached resistive loads does not require a high tolerance. For instance, a higher tolerance in selecting  $R_{l1}$  for R2 and R4 patterns is required as compared to selecting  $R_{l2}$  as shown in Figs. 4(a) and 4(c). Unlike the R2 and R4, R3 allows for less tolerance in  $R_{l1}$  as compared to  $R_{l2}$ .

It is not possible to evaluate the electrode patterns only using the system efficiency that was previously examined. For piezoelectric actuators, the input power is a significant factor. Figure 5(a) depicts the calculated input active power of the first four vibration modes by employing the three electrode patterns shown in Fig. 1(c) and comparing it to the full electrode configuration case. As can be seen in Fig.5(a), electrode patterning considerably boosts active power. Additionally, it should be mentioned that vibration modes with higher

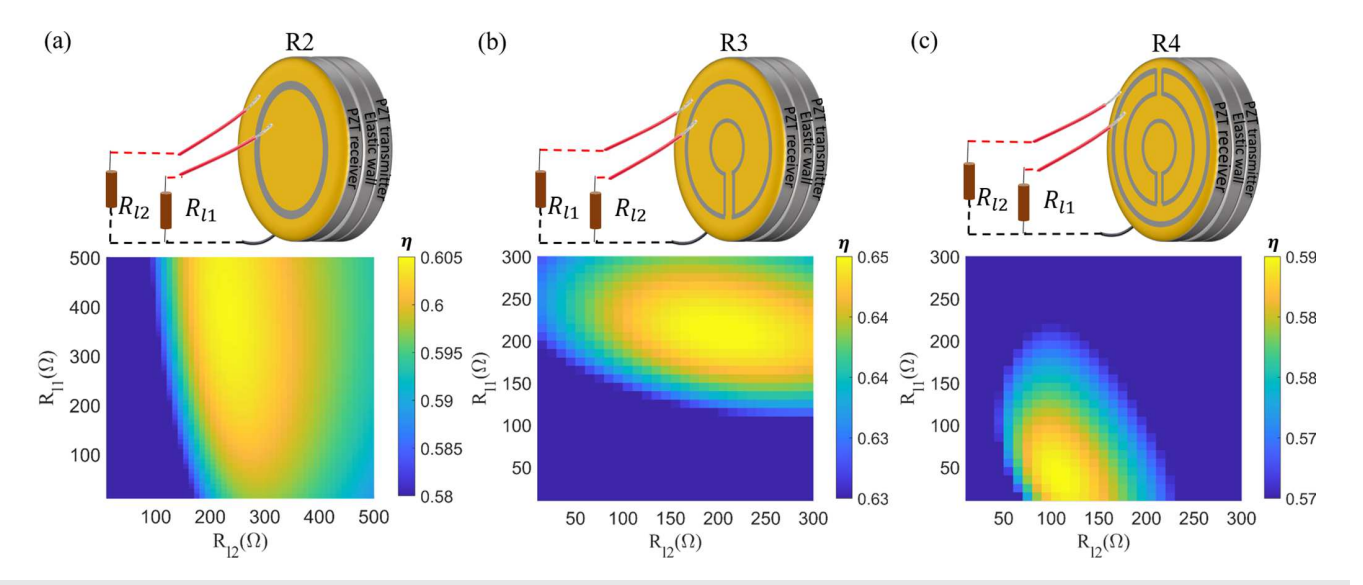


**FIG. 4.** Changes in the system's efficiency when using the resistive loads  $R_{l1}$  and  $R_{l2}$  at the (a) second, (b) third, and (c) fourth radial modes, respectively, while using R2, R3, and R4 electrode configuration.

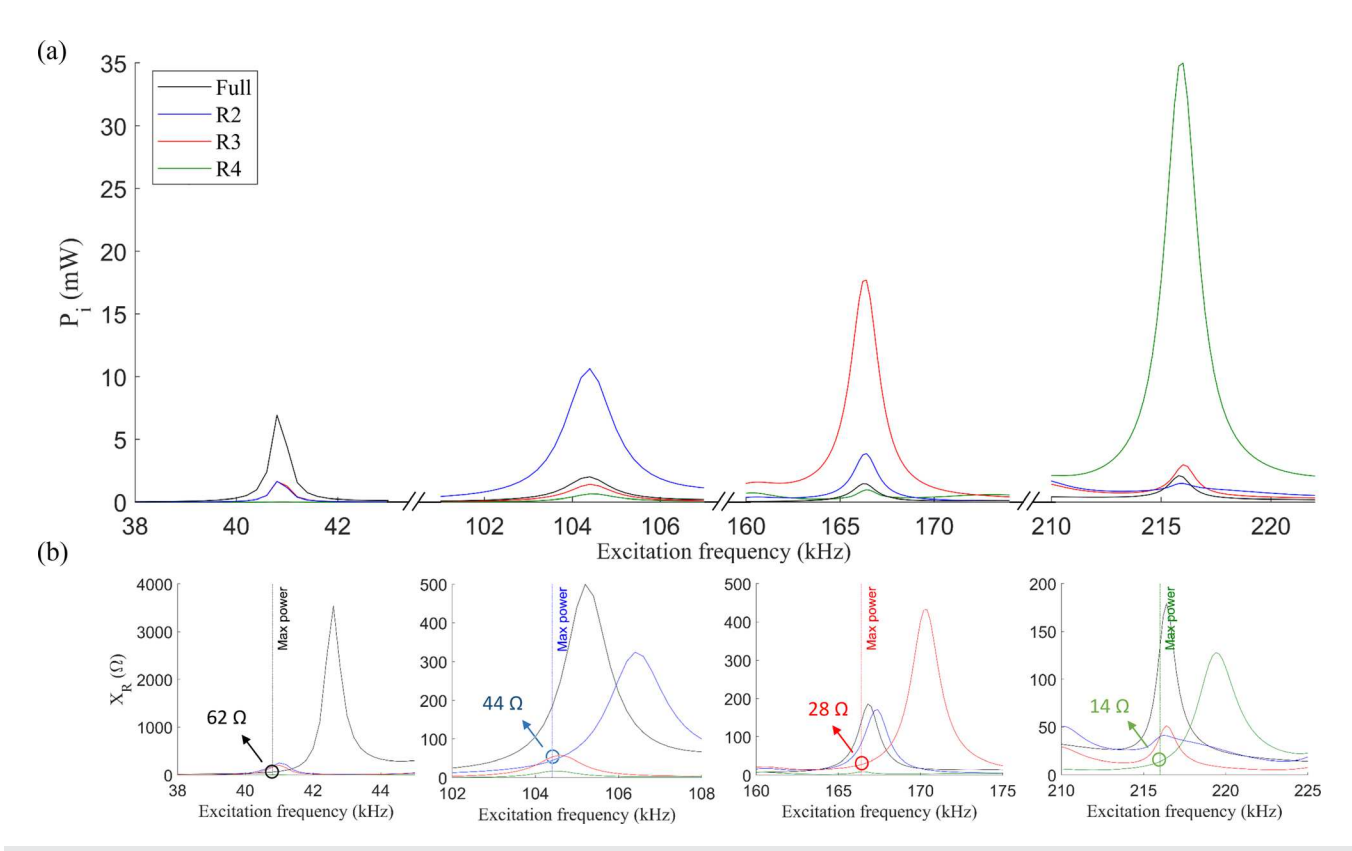


**FIG. 5.** FEM simulation results of (a) the transmitter's input active power in various electrode configurations. For a better representation of modal power, a broken x axis is used to eliminate unneeded areas of the figure. (b) The system's resistance ( $X_R$ ) for the TWUPT system in various electrode configurations. Each subplot in (b) corresponds to its above part of the power plot in (a).

frequencies have more active power. When the input active power equation is taken into consideration, such behavior can be explained as  $P_i = (V_{in}p_f)^2/2X_R$ , where  $p_f$  denotes the power factor. Clearly, two parameters affect the input active power, namely, power factor  $(p_t)$ and system's resistance  $(X_R)$ . Power factor is defined as the ratio of real or active (dissipated) power to apparent (available) power and it is a measure of how in phase the input current is with the input voltage. It is expressed as  $p_f = (|Re(I_{t1})| + |Re(I_{t2})|)/(|I_{t1}| + |I_{t2}|)$ . Electrode patterning results in a significant enhancement in the power factor at the target mode allowing for  $p_f \approx 1$ . This is depicted in the highlighted regions in Figs. 6(a)-6(c) using FEM and experimentally in Figs. 6(d)-6(f). It is worth mentioning that a shunt inductor in series or parallel is commonly used to compensate for the TWUPT system's capacitance, hence increasing the power factor.<sup>29</sup> On the other hand, the system's resistance is expressed as  $X_R = (V_{in}(p_f)^2)/(|Re(I_{t1})|$  $+|Re(I_{t2})|$ ). It can be noted from Fig. 5(b) subplots that as the frequency increases, the system resistance  $(X_R)$  reduces at the location of the maximum power, enabling higher input active power at the higher order modes. The intersection between the vertical line (max power line) with the resistance curve shows decreasing values of 62, 44, 28, and 14  $\Omega$  for the first, second, third, and fourth radial modes, respectively. This explains why active power rises with frequency, as shown in Fig. 5(a). It is vital to note that the power factor augmentation at the target mode comes together with a fall in the power factor associated with the other vibration modes. For instance, the R2 electrode layout boosts the power factor of the second radial mode while decreasing the power factor of the first radial mode as seen in Figs. 6(a) and 6(d). A similar tendency is observed with the system's efficiency which maximizes at the considered modes and declines at the remaining modes. Such behavior permits the use of the TWUPT systems in filtering applications. <sup>18,19</sup>

In conclusion, we evaluated the impacts of electrode patterning on the dynamics of TWUPT systems, as an example of multiplex electromechanical structures, operating at high-order vibration modes. The unique features of TWUPT systems enable differential excitation on the transmitter side while measuring transmitted power and efficiency on the receiving side at different vibration modes. Numerical analysis was used to compute the stress distribution of the studied modes, and electrode patterns were designed and applied to the transmitter and receiver disks. The designed structures were fabricated and corroborated with experiments demonstrating the physical causes of the improved performance due to the use of electrode patterning. The efficiency and active power of the system were computed and tested for the second, third, and fourth radial vibration modes using R2, R3, and R4 electrode patterns, then compared to the full electrode configuration system. We observed that the major reasons for the increase in efficiency are the charge and force cancelation. Both factors contribute to the increase in the quality and power factors of the system. The associated suppression of the other modes facilitates the use of electrode patterning on TWUPT devices in filtering applications.

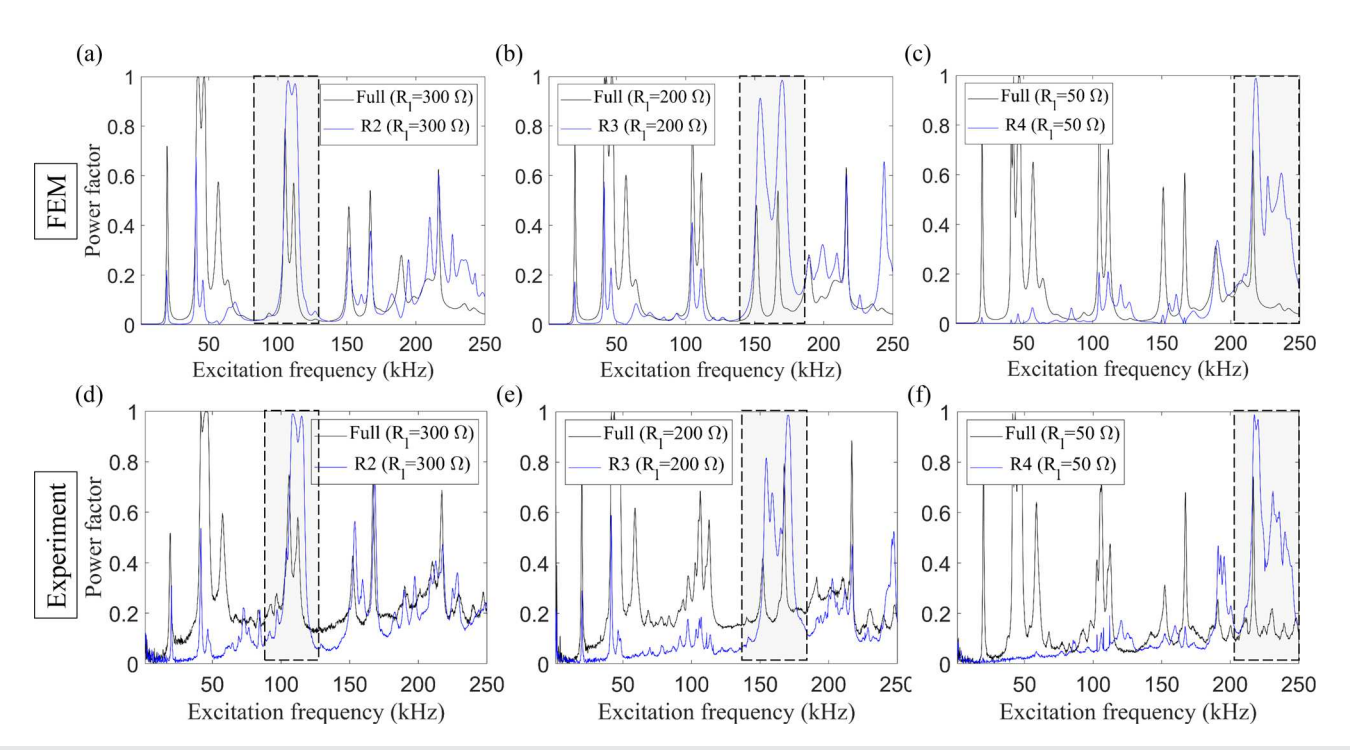


**FIG. 6.** Power factor,  $p_f$  of the TUWPT system with regard to the excitation frequency. Plots (a)–(c) show FEM results, whereas (d)–(f) show the experimental data. The areas that are shaded display the modes of interest.

This work was supported by the U.S. National Science Foundation (NSF) under Grant Nos. ECCS 171113 and CAREER CMMI 2121933, which are gratefully acknowledged.

# AUTHOR DECLARATIONS Conflict of Interest

The authors have no conflicts to disclose.

## **Author Contributions**

Moustafa Sayed Ahmed: Conceptualization (equal); Data curation (lead); Formal analysis (lead); Investigation (lead); Methodology (lead); Software (lead); Validation (lead); Visualization (lead); Writing – original draft (lead); Writing – review & editing (equal). Shima Shahab: Conceptualization (equal); Funding acquisition (lead); Investigation (equal); Project administration (lead); Resources (lead); Supervision (lead); Writing – review & editing (equal).

### DATA AVAILABILITY

The data that support the findings of this study are available from the corresponding author upon reasonable request.

#### **REFERENCES**

- <sup>1</sup>S. Shahab and A. Erturk, "Contactless ultrasonic energy transfer for wireless systems: Acoustic-piezoelectric structure interaction modeling and performance enhancement," Smart Mater. Struct. 23(12), 125032 (2014).
- <sup>2</sup>S. Shahab, M. Gray, and A. Erturk, "Ultrasonic power transfer from a spherical acoustic wave source to a free-free piezoelectric receiver: Modeling and experiment," J. Appl. Phys. 117(10), 104903 (2015).

- <sup>3</sup>A. Sallam, V. C. Meesala, M. R. Hajj, and S. Shahab, "Holographic mirrors for spatial ultrasound modulation in contactless acoustic energy transfer systems," Appl. Phys. Lett. 119(14), 144101 (2021).
- <sup>4</sup>A. Sallam and S. Shahab, "On nonlinear effects in holographic-modulated ultrasound," Appl. Phys. Lett. **121**(20), 204101 (2022).
- <sup>5</sup>M. Bakhtiari-Nejad, A. Elnahhas, M. R. Hajj, and S. Shahab, "Acoustic holograms in contactless ultrasonic power transfer systems: Modeling and experiment," J. Appl. Phys. **124**(24), 244901 (2018).
- <sup>6</sup>Y. Hu, X. Zhang, J. Yang, and Q. Jiang, "Transmitting electric energy through a metal wall by acoustic waves using piezoelectric transducers," IEEE Trans. Ultrason. Ferroelectr. Freq. Control 50(7), 773–781 (2003).
- <sup>7</sup>X. Wang, Z. Shi, and G. Song, "Analytical study of influence of boundary conditions on acoustic power transfer through an elastic barrier," Smart Mater. Struct. 28(2), 025004 (2018).
- <sup>8</sup>M. Sayed Ahmed, M. Ghommem, and S. Shahab, "Mode couplings in multiplex electromechanical structures," J. Appl. Phys. 132(12), 124901 (2022).
- plex electromechanical structures," J. Appl. Phys. **132**(12), 124901 (2022). <sup>9</sup>D. J. Graham, J. A. Neasham, and B. S. Sharif, "Investigation of methods for data communication and power delivery through metals," IEEE Trans. Indus. Electron. **58**(10), 4972–4980 (2011).
- 10 C. U. Grosse, M. Ohtsu, D. G. Aggelis, and T. Shiotani, Acoustic Emission Testing: Basics for Research—Applications in Engineering (Springer Nature, 2021)
- <sup>11</sup>E. F. Crawley and J. D. Luis, "Use of piezoelectric actuators as elements of intelligent structures," AIAA J. 25(10), 1373–1385 (1987).
- <sup>12</sup>A. Erturk, P. A. Tarazaga, J. R. Farmer, and D. J. Inman, "Effect of strain nodes and electrode configuration on piezoelectric energy harvesting from cantilevered beams," J. Vib. Acoust. 131(1), 011010 (2009).
- <sup>13</sup>C.-K. Lee and F. C. Moon, "Modal sensors/actuators," J. Appl. Mech. 57, 434–441 (1990).
- <sup>14</sup>J. S. Pulskamp, S. S. Bedair, R. G. Polcawich, G. L. Smith, J. Martin, B. Power, and S. A. Bhave, "Electrode-shaping for the excitation and detection of permitted arbitrary modes in arbitrary geometries in piezoelectric resonators," IEEE Trans. Ultrason. Ferroelectr. Freq. Control 59(5), 1043–1060 (2012).

- 15T. Matsumura, M. Esashi, H. Harada, F. Thalmayr, K.-y. Hashimoto, and S. Tanaka, "Selective mode excitation of piezoelectric disk-type resonator by electrode pattern definition," in *IEEE International Ultrasonics Symposium* (IEEE, 2010), pp. 979–982.
- 16 A. Prak, M. Elwenspoek, and J. H. Fluitman, "Selective mode excitation and detection of micromachined resonators," J. Microelectromech. Syst. 1(4), 179–186 (1992).
- <sup>17</sup>H. A. Tilmans, D. J. IJntema, and J. H. Fluitman, "Single element excitation and detection of (micro-) mechanical resonators," in *Proceedings of International Conference on Solid-State Sensors and Actuators (TRANSDUCERS'91)*, San Francisco, CA (IEEE, 1991), pp. 533–537.
- <sup>18</sup> A. Elka and I. Bucher, "Optimal electrode shaping for precise modal electromechanical filtering," Struct. Multidiscip. Optim. 38(6), 627–641 (2009).
- <sup>19</sup>J. Sanchez-Rojas, J. Hernando, A. Donoso, J. Bellido, T. Manzaneque, A. Ababneh, H. Seidel, and U. Schmid, "Modal optimization and filtering in piezoelectric microplate resonators," J. Micromech. Microeng. 20(5), 055027 (2010).
- <sup>20</sup>S. Sherrit, S. P. Leary, B. P. Dolgin, and Y. Bar-Cohen, "Comparison of the Mason and KLM equivalent circuits for piezoelectric resonators in the thickness mode," in *IEEE Ultrasonics Symposium (Cat. No. 99CH37027)* (IEEE, 1999), Vol. 2, pp. 921–926.
- <sup>21</sup>S. Sherrit, M. Badescu, X. Bao, Y. Bar-Cohen, and Z. Chang, "Efficient electromechanical network model for wireless acoustic-electric feed-throughs," Proc. SPIE 5758, 362–372 (2005).

- <sup>22</sup>X. Bao, B. J. Doty, S. Sherrit, M. Badescu, Y. Bar-Cohen, J. Aldrich, and Z. Chang, "Wireless piezoelectric acoustic-electric power feedthru," Proc. SPIE 6529, 652940 (2007).
- <sup>23</sup>K. Wilt, H. Scarton, S. Roa-Prada, G. Saulnier, J. Ashdown, T. Lawry, P. Das, and A. Gavens, "Finite element modeling and simulation of a two-transducer through-wall ultrasonic communication system," ASME Int. Mech. Eng. Congr. Expo. 43888, 579–589 (2009).
- <sup>24</sup>M. A. S. Ahmed, B. Robert, M. Ghommem, and S. Shahab, "Genetic algorithm optimization for through-wall ultrasound power transfer systems," Proc. SPIE PC12043, Active and Passive Smart Structures and Integrated Systems XV (2022).
- 25 R. L. Lin, F. C. Lee, E. M. Baker, and D. Y. Chen, "Inductor-less piezoelectric transformer electronic ballast for linear fluorescent lamp," in Sixteenth Annual IEEE Applied Power Electronics Conference and Exposition (Cat. No. 01CH37181) (APEC 2001) (IEEE, 2001), Vol. 2, pp. 664–669.
- <sup>26</sup>A. Bhargava, V. C. Meesala, M. R. Hajj, and S. Shahab, "Nonlinear effects in high-intensity focused ultrasound power transfer systems," Appl. Phys. Lett. 117(6), 064101 (2020).
- <sup>27</sup>V. C. Meesala, M. R. Hajj, and S. Shahab, "Analysis and prediction of shock formation in acoustic energy transfer systems," J. Appl. Phys. 128(23), 234902 (2020).
- <sup>28</sup>T. Lawry, K. Wilt, S. Roa-Prada, J. Ashdown, G. Saulnier, H. Scarton, P. Das, and J. Pinezich, "Electrical optimization of power delivery through thick steel barriers using piezoelectric transducers," Proc. SPIE 7683, 216–227 (2010).
- <sup>29</sup>S. Lin and J. Xu, "Effect of the matching circuit on the electromechanical characteristics of sandwiched piezoelectric transducers," Sensors 17(2), 329 (2017).